Electrostatics in the Stability and Misfolding of the Prion Protein: Salt Bridges, Self-Energy, and Solvation

Will Guest[1], Neil Cashman[1,3], and Steven Plotkin[2,3]

April 12, 2010

[1]Brain Research Centre, University of British Columbia, V6T 2B5
[2]Department of Physics and Astronomy, University of British Columbia, V6T 1Z1
[3]Corresponding authors (Email: neil.cashman@vch.ca, steve@physics.ubc.ca, Phone: 1-604-822-2135, 1-604-822-8813)

1

Abstract

Using a recently developed mesoscopic theory of protein dielectrics, we have calculated the salt bridge energies, total residue electrostatic potential energies, and transfer energies into a low dielectric amyloid-like phase for 12 species and mutants of the prion protein. Salt bridges and self energies play key roles in stabilizing secondary and tertiary structural elements of the prion protein. The total electrostatic potential energy of each residue was found to be invariably stabilizing. Residues frequently found to be mutated in familial prion disease were among those with the largest electrostatic energies. The large barrier to charged group desolvation imposes regional constraints on involvement of the prion protein in an amyloid aggregate, resulting in an electrostatic amyloid recruitment profile that favours regions of sequence between alpha helix 1 and beta strand 2, the middles of helices 2 and 3, and the region N-terminal to alpha helix 1. We found that the stabilization due to salt bridges is minimal among the proteins studied for disease-susceptible human mutants of prion protein.

Introduction

Misfolded prion protein is the causative agent for a unique category of human and animal neurodegenerative diseases characterized by progressive dementia, ataxia, and death within months of onset (Prusiner 1998). These include Creutzfeldt-Jakob disease (CJD), fatal familial insomnia, and Gerstmann-Sträussler-Scheinker syndrome in humans, bovine spongiform encephalopathy in cattle, scrapie in sheep, and chronic wasting disease in cervids. Unlike other infectious conditions that are transmitted by conventional microbes, the material responsible for propagation of prion diseases consists of an abnormally folded conformer of an endogenous protein, possibly in complex with host nucleic acids or sulfated glycans (Caughey et al. 2009). Soluble, natively-folded monomers of the prion protein (known as PrP^C) may adopt an aggregated protease-resistant conformation known as PrP^{Sc} that is capable of recruiting additional monomers of PrP^C and inducing them to misfold in a process of template-directed conversion. This results in ordered multimers of prion protein that, when fractured, act as additional seeds to propagate the misfold through the reservoir of PrP^C present in brain. Although the conversion process may be initiated by an infectious inoculum of PrP^{Sc}, it may also arise spontaneously or due to mutations in the gene coding for PrP that predispose to misfolding.

Structurally, PrP^C is a glycophosphatidylinositol-anchored glycoprotein of 232 amino acids comprising an N-terminal unstructured domain and a C-terminal structured domain of 3 α-helices (hereafter referred to as $\alpha1$, $\alpha2$, and $\alpha3$ in order) and a short two-stranded antiparallel β-sheet (made of strands $\beta1$ and $\beta2$), while PrP^{Sc} has substantially enriched β content speculated to form a stacked β-helix (Govaerts et al. 2004) or extended β-sheet (Cobb et al. 2007) conformation in the amyloid fibril.

At a molecular level PrP misfolding is a physico-chemical process, with the propensity to misfold determined by the free energy difference between folded and misfolded states and the magnitude of the energy barrier separating them. As in any protein system, electrostatic effects make significant contributions to the energies of the various states and take two forms: salt bridge energy due to spatial proximity of charged groups within the native protein, and solvation/self energy due to field energy storage in the ambient protein and water dielectric media. *A priori*, it is expected that electrostatic effects generally favour the well-solvated monomeric PrP^C over the more hydrophobic amyloid PrP^{Sc}, since formation of PrP^{Sc} necessitates disruption of salt bridges in the native structure (although this may be compensated for by the formation of alternative salt bridges in PrP^{Sc}) and transfer of some charged groups into an environment of lower permittivity, both of which are energetically costly. However, these penalties on formation of PrP^{Sc} are counterbalanced by hydrogen bonding, hydrophobic, and possibly entropic contributions that favour the amyloid form (Tsemekhman et al. 2007). Regional variation in the electrostatic transfer energy to water and amyloid may be useful in

predicting participation in the amyloid core of PrP^{Sc}. Furthermore, several of the causative mutations for familial prion disease involve substitution of charged residues for uncharged residues (such as the D178N mutation responsible for fatal familial insomnia or familial CJD, depending on mutant allele polymorphism status at codon 129) or charge reversal of a residue (such as E200K, the most common mutation in classical familial CJD) (Kovacs et al. 2002), offering an indication of the importance of electrostatic effects in the misfolding process. More broadly, it has been found that changes in the charge state of a mutant protein compared to wild-type relate to its tendency to form aggregates (Chiti et al. 2003), and the aggregation propensity of a polypeptide chain is inversely correlated with its net charge (Chiti et al. 2002); similarly, aggregation propensity is maximal at the protein iso-electric point where the net charge is zero (Schmittschmitt and Scholtz 2003). Intrinsically unstructured proteins tend to have a high net charge (Uversky, Gillespie and Fink 2000), which increases the electrostatic cost for the system to condense into the folded structure. Sequence correlations between charged groups may affect the kinetics of amyloid formation as well (Dima and Thirumalai 2004).

The role of salt bridges in prion disease has been investigated previously by molecular dynamics simulation (MDS) and experimental studies of mutant protein. MDS of human PrP^{C} has identified salt bridges that play a role in stabilization of the native structure (Zuegg and Gready 1999). Other MDS studies of the R208H mutation, which disrupts a salt bridge with residues D144 and E146 of α-helix 1, have shown that it results in global changes to the backbone structure (Bamdad and Naderi-Manesh 2007). Experimentally, the E200K mutant of PrP^{C} has been shown through calorimetry to be 4 kJ/mol less stable than wild type (Swietnicki et al. 1998). Mutation of two aspartates participating in $\alpha1$ intra-helix salt bridges to neutral residues increases misfolding fourfold in cell-free conversion reactions under conditions favouring salt bridge formation (Speare et al. 2003). Interestingly, complete reversal of charges in $\alpha1$ appears to inhibit conversion, possibly by preventing docking of PrP^{C} and PrP^{Sc} (Speare et al. 2003). The pH dependence of charge interactions in PrP^{C} has also been investigated to identify those most sensitive to pH changes (Warwicker 1999); this is an important aspect of the problem because of the observed increased PrP^{C} misfolding rate at low pH.

A unifying analysis of all PrP^{C} salt bridges would be useful in understanding their role in structural stability. As well, to our knowledge solvation energy contributions to the misfolding process have not yet been investigated; they would offer a helpful perspective for probing the propensity of different regions of the prion protein to participate in the PrP^{Sc} amyloid core.

Direct extraction of salt bridge and solvation energies from molecular dynamics is complicated by the need to run long-length simulations that sample the equilibrium between states of interest, which can be

prohibitively slow for states that differ significantly in energy. An alternative approach is to use a continuum electrostatics description of the protein-water system, in which the response of surrounding material is modelled through solution of the Poisson-Boltzmann equation as a macroscopic dielectric that varies from a low value (usually 4) within the volume of the protein to 78 (the dielectric constant of bulk water) outside the protein. The downside of this method is that it ignores subtleties of the protein response to perturbing fields, such as cooperative internal reorganization. Using results from Kirkwood-Frölich theory (Oster and Kirkwood 1943; Frohlich 1949; Voges and Karshikoff 2000), we have recently developed a procedure to compute a spatially-varying dielectric function for a protein based on fluctuation statistics obtained from brief equilibrium MD simulations that capture much of the microscopic response of the protein at moderate computational cost (Guest et al. 2009). This provides a convenient tool to calculate solvation and salt bridge energies for all residues in a protein from a single simulation. In what follows we apply this method to determine the energies for all salt bridges in 12 molecular species of prion protein and the transfer energy for all residues in these proteins into a hypothetical protein amyloid core.

Methods

Twelve structures of various species and mutants of PrP^C were selected from the Protein Data Bank (PDB), including the species human 1QLZ and 1QLX (Zahn et al. 2000), cow 1DX0 (Lopez Garcia et al. 2000), turtle 1U5L, frog 1XU0, chicken 1U3M (Calzolai et al. 2005), mouse 1AG2 and 1XYX (Riek et al. 1996; Gossert et al. 2005), dog 1XYK, pig 1XYQ, cat 1XYJ (Lysek et al. 2005), wallaby 2KFL (Christen et al. 2009) and the human mutants D178N 2K1D (Mills et al. 2009) and E200K 1FKC (Zhang et al. 2000). They were taken as starting points for 5ns all-atom molecular dynamics simulations using the CHARMM force field version C31B1 (Brooks et al. 1983) with explicit pure solvent water (no salt), periodic boundary conditions, particle mesh Ewald electrostatics, a timestep of 2fs, and a Lennard-Jones potential cutoff distance of 13.5Å. The basic residues (ARG and LYS) were protonated, while the acidic residues (HIS, ASP, and GLU) were deprotonated to reflect ionization conditions at pH 7. The system was first minimized for 200 time steps before starting the simulation. Snapshots of the simulations were taken every 2ps to build up an ensemble of equilibrium conformations for each protein. The dipole moments μ of all residue side chains and backbones were calculated at each snapshot and used to obtain the correlation coefficients

$$R_{ij} = \frac{\langle \mu_i \mu_j \rangle}{\sqrt{\langle \mu_i^2 \rangle \langle \mu_j^2 \rangle}} \tag{1}$$

for all pairs of Cartesian dipole components μ_i and μ_j, where the angle brackets denote an average over all snapshots (the thermal average). The matrix R of correlation coefficients was diagonalized to isolate the normal modes of dipole fluctuations, which describe the response of charged groups to perturbations around equilibrium. The R matrix for each protein was used to calculate the local dielectric map (Guest et al. 2009). See Figure 1 in the Supplementary Material for the dielectric map of human PrP. These dielectric maps were then taken as input for the Poisson-Boltzmann solver APBS (Baker et al.2001) to solve the linearized Poisson-Boltzmann equation on an 97^3 mesh in 150 mM NaCl, again with periodic boundary conditions, to obtain the electrostatic energies required below. Atomic radii were assigned according to the CHARMM force field by the program PDB2PQR (Dolinsky et al. 2004). The often-used simplifying approximation of a constant internal protein dielectric constant of 4 and water dielectric constant of 78 was employed for comparison (Kumar and Nussinov 1999).

Salt bridges in the set of proteins were identified by searching all pairs of charged atoms for those with charged groups within 12Å of each other, whether the charges were alike or different. The energy of each salt bridge was determined by a mutation cycle designed to isolate the charge interaction energy from the energy in the surrounding dielectric milieu as shown in Figure 1. For charged groups A and B, their salt bridge energy E_{sb} was taken to be a function of the energy of the protein system with both charges in place, E_{AB}, with one or the other charge removed, E_A and E_B, and with both charges removed, E_0, as follows:

$$E_{sb} = E_0 + E_{AB} - (E_A + E_B). \tag{2}$$

Here, E_0 contains only the self energy of the part of the protein not including A and B (labelled P in Figure 1), while E_{AB} contains the self energies of A, B, and P as well as the pairwise interaction energies between A and B, A and P, and B and P. E_A contains the self energies of A and P and their interaction energies (E_B is analogous). Combining the terms as shown causes all the energies except the interaction energy of A and B to cancel.

Another cycle, also shown in Figure 1, was used to determine the total contribution of each residue to the electrostatic energy of the protein, E_{elec}. For each side chain in the protein, the electrostatic energies of the side chain E_{sc} and the protein lacking the side chain $E_{whole-sc}$ were calculated in isolation in the protein dielectric environment and subtracted from the electrostatic energy of the intact protein E_{whole}:

$$E_{elec} = E_{whole} - E_{sc} - E_{whole-sc}. \tag{3}$$

The terms E_{sc} and $E_{whole-sc}$ contain the self energies of the side chain and rest of the protein respectively, and E_{whole} contains these self energies as well as the interaction energy of the side chain with the rest of the protein. Subtracting the terms as shown causes the self energies to cancel, leaving only the interaction energy between the side chain and the protein. This energy can be thought of as the electrostatic potential energy of a residue in the protein.

To approximate the electrostatic energy of residue transfer into a hydrophobic, low dielectric environment like the core of a PrP^{Sc} amyloid, the energy $E(\epsilon_{PrPC})$ of a residue in the dielectric environment of PrP^{C} was compared to the energy $E(\epsilon_{PrPSc})$ of the residue in a homogeneous dielectric of $\epsilon = 4$, which describes the dielectric response in the interior of a bulk amyloid protein phase. Since the nature of monopole fields in the PrP^{Sc} structure is unknown, interactions between charged residues are omitted from the calculation, so the transfer energy reflects only changes in the dielectric environment. For a given residue, the dielectric contribution to the transfer energy E_{trans} is:

$$E_{trans} = E(\epsilon_{PrP^{Sc}}) - E(\epsilon_{PrP^{C}}). \tag{4}$$

Results

Dynamics of Dipoles at Equilibrium

The modes obtained by diagonalizing the correlation matrix R in Equation 1 generally involved several parts of the molecule; correlations were not limited to residues close in space or sequence. This is consistent with phonon transmission of perturbations at one site throughout the molecule by strong steric coupling effects through solid-like elastic moduli. The four largest-amplitude dipole modes for human PrP are shown in Figure 2. Dipole fluctuations were not qualitatively different between species, but different regions of the molecule exhibited characteristic motions. The two long alpha helices 2 and 3 exhibited primarily synchronous motion, with the helices rocking back and forth together as a unit. Nonetheless, some dipoles in the helices exhibited contrary motion. Alpha helix 1 did show some autonomy from the rest of the structure and tended to fluctuate as a group.

Motion of the beta sheet is prominent in several of the modes. Two patterns stand out: a see-saw motion in which one strand tilts up as the other tilts down with both strands pivoting about the middle of the strands, and an in-out motion in which the outer beta strand ($\beta1$) and the N-terminal part of $\alpha2$ move synchronously away from the inner beta strand ($\beta2$). The first motion is seen in modes 2 and 3 in Figure

7

2 above, while the second motion is seen in other lesser-amplitude modes. This is compatible with NMR observations of the beta sheet, which show slow exchange between a range of conformations (Liu et al. 1999; Viles et al. 2001). In the NMR experiments, motion of the beta strands was observed on a time scale of microseconds, while these simulations only spanned nanoseconds, but both are indicative of some degree of conformational flexibility in the beta sheet.

Salt bridge energies

The PrP structures analysed contained a diverse set of salt bridges, ranging from moderately attractive to weakly repulsive. A complete list of salt bridges in all structures is presented in Table 1 of the Supplementary Material; salt bridges in the human structure are shown in Table 1 for both the single NMR structure 1QLX and the ensembe of 20 NMR structures 1QLZ.

Structurally, the salt bridges can be divided into local and nonlocal by the proximity in sequence of the participating residues. Local salt bridges, like Asp148—Glu152 in $\alpha 1$, Asp208—Glu211 in $\alpha 3$, and Arg164—Asp167 between $\beta 2$ and the following loop serve to stabilize secondary structural elements of the protein, while nonlocal salt bridges like Arg156—Glu196, Arg164—Asp178, and Glu146—Lys204 help to hold these elements together in the overall tertiary fold. Figure 3 shows the position of these nonlocal salt bridges in bovine PrP.

Many of the salt bridges identified were near the protein surface, where the high degree of solvation attenuates their strength; the strongest salt bridges were those best sequestered from solvent, for this places them in a dielectric environment that increases electric field strength. The strongest salt bridge of all, between residues 206 and 210 of frog PrP, features a special "two-pronged" geometry that enables the amino group of Lys 210 to associate with both carboxyl oxygens on Asp 206. Interestingly, two strong but intermittant salt bridges are present in human 1QLZ between the C-terminal arginine and residue 167 in the $\beta 2 - \alpha 2$ loop and residue 221 in $\alpha 3$. The substantial variation between members of the NMR ensemble at the C-terminus results in large motion of the arginine side chain, so that these salt bridges are only formed in a subset of conformers. Similarly, the ARG 164 - ASP 178 salt bridge that helps to anchor the beta sheet to $\alpha 2$ and $\alpha 3$ is not present in all members of the 1QLZ NMR ensemble, although it is quite strong in the single 1QLX structure. Although attractive salt bridges predominate, there were a number of repulsive salt bridges identified as seen on the left hand side of Figure 5A, especially in $\alpha 1$ and $\alpha 3$, which are crowded with several charged residues. As demonstrated in the following section, despite the presence of these destabilizing interactions, no residue experiences a net repulsive potential as these unfavourable salt

8

bridges are counterbalanced by the presence of other, stronger, favourable ones. The total energies due to all salt bridges in each molecular species studied are shown in Figure 5B. Of note is the much reduced total salt bridge energy in the two human mutants, E200K and D178N, compared to any other structure. The categorization of species as susceptible or resistant to prion disease is somewhat approximate, but comparison of total salt bridge energy and disease susceptibility by Kendall's tau gives a value of $\tau = 0.45$, implying that the order of species by salt bridge energy and disease susceptibility are significantly concordant (p = 0.046). Overall, the effect of a heterogeneous dielectric was to moderate putatively strong salt bridges under the biphasic protein-water approximation for the dielectric function.

The salt bridges listed in Table 1 of the Supplementary Material are those present at pH 7, but for human PrP an additional search was performed to identify salt bridges that would emerge at lower pH, since acidic conditions are known to drive PrP^{Sc} formation. Lower pH results in protonation of histidine residues to produce a positively charged species, which in human PrP enables the formation of three additional weakly attractive salt bridges (indicated by daggers in Table 1). While the dominant effect of lowering pH is to reprotonate acidic side chains, thus reducing electrostatic stability, this is partially compensated for by the formation of salt bridges involving histidine.

Total residue electrostatic energies

The salt bridge energies describe pairwise effects, but for mutational analysis it is more important to know the total contribution of each side chain to the stability of the protein. These energies approximate the electrostatic contribution to the energy change on mutation to a residue with a small nonpolar side chain like alanine. In practice, the side chain of each residue is removed from the protein. The total electrostatic energy of each residue in all prion proteins studied was less than or equal to 0, indicating a strong degree of evolutionary selection toward residues that benefit stability in the folded conformation. Through electrically neutral, or nearly so, proteins have their internal dipoles oriented so as to lower the potential energy of every residue. In human PrP, it is instructive to correlate the energies to known pathogenic mutations: the residue with the greatest overall stabilizing energy, Thr183, is implicated in familial CJD by a T183A mutation (Kovacs et al. 2002); this mutation has also been shown to radically reduce measured stability by urea denaturation (Liemann and Glockshuber 1999). It is interesting to note that this residue, although not charged, is polar and more deeply buried in the hydrophobic core of the protein than any other charged residue, thereby enhancing the effect of dipolar attractions with its neighbors. Other residues that on mutation cause familial prion disease have especially high total electrostatic stabilizing energies, including

D178 and D202. Table 3 gives the 10 human side chains with the greatest total electrostatic energies. We might anticipate that mutation of other residues in Table 3 may enhance the probability of developing misfolding-related disease.

Transfer to hydrophobic environment

In forming the amyloid core of PrP^{Sc}, some residues must undergo the migration to a region of low dielectric constant. For highly charged residues, this transfer energy is prohibitively high and may thereby exclude their participation in the amyloid core, while for nonpolar residues the small electrostatic transfer energy cost is overcome by favourable solvation entropy changes. By mapping the transfer energy of each residue into a region of low dielectric approximating PrP^{Sc} amyloid, it is possible to predict the likelihood of recruitment for various PrP regions into the amyloid core, without the aid of specific dipole-dipole correlations as might be present in the amyloid. Figure 6 shows the transfer energy from the PrP^{C} dielectric to a homogeneous dielectric of 4 for various species of PrP^{C}. The transfer energy to an aqueous environment would show an inverse pattern. A 7 amino acid summing window is applied because sequence heterogeneity causes large variation between adjacent residues, and individual residues cannot enter the amyloid core without placing their neighbors in it as well. The transfer energies in Figure 6 are quite large, but including other terms in addition to the electrostatic energies considered here will reduce the magnitude of the total transfer free energy.

There is considerable variation in the transfer energy along the sequence, with the lowest barrier to dielectric transfer for the region between $\alpha1$ and $\beta2$, the middles of $\alpha2$ and $\alpha3$, and $\beta1$. Conversely, $\alpha1$, the loop between $\beta2$ and $\alpha2$, and the loop between $\alpha2$ and $\alpha3$ show a formidable barrier to transfer. This overall pattern is well preserved among all PrP structures studied (see Supplementary Material Figure 4). Immunological studies have defined $\beta2$ as a PrP^{Sc}-specific epitope (Paramithiotis et al. 2003), which presumably necessitates its surface exposure. In the human structure, $\beta2$ is located at the border between regions of low and high transfer energies, so it is possible that it is close in proximity to the amyloid core but protrudes sufficiently to be recognised by antibodies.

The overall contour of the transfer energy functions is similar for all PrP structures studied, but there is some variation that correlates with known infectivity data. As seen in Figure 6, human and bovine share highly similar transfer energy profiles and are both susceptible to prion disease and interspecies transmission of disease, while non-mammalian turtle PrP that does not form PrP^{Sc} has a different profile, with a higher transfer energy barrier than cow or human over 4/5 of the sequence. PrP^{C} from dog, a mammalian species

known to be resistant to prion infection (Polymenidou et al. 2008), is intermediate between the human and turtle profiles. The average transfer energies correlate with a species' resistance to disease (Figure 6 legend). Some other species, including chicken, turtle, and wallaby, have a qualitatively different transfer energy function.

Discussion

Although electrostatic effects are only one contribution to the enigmatic $PrP^C \to PrP^{Sc}$ conversion process, they offer clues to many of the central questions in prion biochemistry. The spatial variation of the dielectric is important, as neither charge separation distance, dielectric constant at the midpoint of the salt bridge, nor burial can predict salt bridge stability or total electrostatic energy (see Figures 2 and 3 of the Supplementary Material). As shown above, salt bridges play an important role in stabilizing both secondary and tertiary aspects of the PrP^C structure. In fact, the total energy of all salt bridges in human PrP^C is -60 kJ/mol, almost twice the total stability of the protein as determined by calorimetry (Swietnicki et al. 1998; Liemann and Glockshuber 1999). Thus disruption of even a proportion of salt bridges in PrP^C is sufficient to substantially destabilize the folded conformation, possibly accelerating or enabling the transition to PrP^{Sc} in the right conditions. However, as has been observed elsewhere (Hendsch et al. 1996), the free energy change of salt bridge disruption may not be equal to the Coulombic energy of the salt bridge itself, due to the competing favourable reduction in desolvation energy. This will partially offset the change in stability from salt bridge disruption. Charge interactions may also participate in the poorly-understood association between the unstructured N-terminal domain and structured C-terminal domain of PrP^C. As shown previously, the C-terminal domain organization depends on the length of N-terminal tail present (Li et al. 2009), possibly through a collection of transient interactions below the detection threshold of NMR, resulting in an "avidity-enhanced" C-terminal structure. Charge complementarity between the N- and C-terminal domains provides one explanation for this phenomenon. For example, the very N-terminus of PrP^C contains the highly positively charged region KKRPK from codons 25–29, while $\alpha 1$ contains the highly negatively charged region DYED from codons 144–147. If the N-terminal tail is free to explore a random walk around the C-terminal domain, electrostatic attractions are likely to bias this part of the tail toward residence near $\alpha 1$, a region that is especially influenced by the length of tail present. The net attraction between the N-terminal tail and C-terminal structure may be insufficient to structure the tail but sufficient to collapse or condense the tail onto the surface of the structured domain, resulting in a kind of "molten shell." Further exploration of

this phenomenon, by molecular dynamics or other tools, may prove insightful.

The importance of acidic conditions in the PrP conversion has been known for some time (Hornemann and Glockshuber 1998), and acidity exerts a large effect through modification of the protonation states of charged residues. At slightly acidic pH below the pKa of histidine (6.5), protonation of the histidine imidazole ring creates mildly stabilizing salt bridges with nearby residues. In the prion literature, histidines are a subject of considerable attention for their ability to coordinate copper ions in the octapeptide repeat region of the N-terminal domain (Aronoff-Spencer et al. 2000; Viles et al. 2008), but it seems that they also help to protect PrP$^{\mathrm{C}}$ from the stress of mildly acidic conditions. At much lower pH, however, protonation of glutamate and aspartate side chains ablates some of the stabilizing salt bridges shown in Table 1, which substantially reduces the energy barrier to rearrangement of PrP$^{\mathrm{C}}$ components. For example, at pH 4.5, the pKa predictor program PROPKA (Bas et al. 2008) identifies glutamate residues 168, 200, 219, and 221 as being significantly protonated, which will affect the stability of the protein and whose systematic investigation is a topic for future work. The influence of acidity on the monomeric PrP$^{\mathrm{C}}$ structure has been extensively studied by molecular dynamics (Gu et al. 2003; Langella et al. 2004; DeMarco and Daggett 2007), but perhaps the most noteworthy effect of acidity may not be in the resulting structural transition of the isolated PrP$^{\mathrm{C}}$ monomer but rather in lowering the barrier to induced reorganization in the presence of the templating species.

Another natural question is the role that electrostatics play in the formation of the PrP$^{\mathrm{Sc}}$ amyloid. It may be argued that since the transfer energy profile in Figure 6 neglects the possibility of forming strong salt bridges in the low dielectric amyloid core of PrP$^{\mathrm{Sc}}$ it misrepresents the ability of these charges to stably occupy the amyloid. A counterexample may be constructed in a case of homogeneous dielectrics. The total energy change ΔE_{total} on bringing two opposite charges A and B both of charge q and radius r_{ion} from a large distance apart in a medium with high dielectric ϵ_{solv} like water into close proximity r_{AB} in a region of low dielectric ϵ_{prot} to form a salt bridge is equal to the sum of the solvation energy changes ΔE_{solv}^{A} and ΔE_{solv}^{B} and their pairwise Coulomb energy ΔE_{AB}. Treating the charges as Born ions, in the limit where $\epsilon_{prot}/\epsilon_{solv} \ll 1$ (a valid assumption since generally $\epsilon_{solv} = 78$ and $\epsilon_{prot} = 4$, so $\epsilon_{prot}/\epsilon_{solv} \approx 0.05$), the total energy change to form the desolvated salt bridge is:

$$\Delta E_{total} = \Delta E_{solv}^{A} + \Delta E_{solv}^{B} + \Delta E_{AB} = 2q^2 \left(\frac{1}{2r_{ion}} \right) \left(\frac{1}{\epsilon_{prot}} - \frac{1}{\epsilon_{solv}} \right) - \frac{q^2}{\epsilon_{prot} r_{AB}} \approx \frac{q^2}{\epsilon_{prot}} \left(\frac{1}{r_{ion}} - \frac{1}{r_{AB}} \right). \quad (5)$$

This is always positive since r_{AB} is greater than r_{ion} to satisfy the stereochemistry of the atoms. Thus

although salt bridges may partially mitigate the burial of charged residues, they cannot alter the fundamental unfavourability of the electrostatic component of this process. It is also possible that solvent-exposed salt bridges may form in the misfolded state outside or on the surface of the amyloid or oligomeric core, which could occur without the desolvation penalty described above. This would provide a mechanism to stabilize charged and polar parts of the protein in the misfolded form. Such salt bridges are likely to be relatively low in energy due to the high ambient dielectric environment, and it has been observed for amyloid-beta 16-22 peptide that hydrophobic forces are more important than specific salt bridges in driving amyloid formation (Ma and Nussinov 2002). However as mentioned above, it has been shown that the net charge of a polypeptide chain incurs resistance to aggregation (Chiti et al. 2002; Schmittschmitt and Scholtz 2003), consistent with the notion of a higher overall energetic cost of transfer into a low dielectric medium for more highly charged polypeptides. In light of this, we believe the transfer energy profiles accurately convey this part of the obstacle to amyloid formation.

Continuum electrostatics as a tool to examine protein behaviour has limitations, namely that it ignores the microscopic response of the system and thereby risks omitting subtle but important effects. However, by deriving the dielectric map from all-atom molecular dynamics simulations of the proteins of interest, we are able to substantially incorporate the microscopic response in our model and thereby improve the reliability of the energy estimates obtained. Previous theories could not reliably predict the effective dielectric constant inside a protein, so values typically between 4 and 10 have been used as initial guesses. Stronger salt bridges in the interior tend to be better predicted by an interior dielectric of 4, which would then overestimate the strength of the more abundant salt bridges on the protein surface. An interior dielectric of 10 best predicts the strength of the abundant surface salt bridges, but would then underestimate the strength of the buried interior salt bridges. The heterogeneous dielectric theory in (Guest et al. 2009) makes it unnecessary to guess at the value of the dielectric inside a protein and also indicates that no single value in the interior is satisfactory. Quantum effects due to electronic polarizability may be added to this approach as further refinement. The conformational variability in the ensemble of NMR structures for each PrP molecule also introduces an inherent uncertainty in the calculation of electrostatic energies, which we treated by averaging salt bridge energies over all NMR ensemble members. The molecular dynamics relaxation methods, often done in the absence of counterions, may introduce uncertainty as well. Electrostatic considerations are relevant to many aspects of the prion question, from PrP^C dynamics and stability to PrP^{Sc} amyloid organization and templating. We have presented an analysis of salt bridge, electrostatic, and hydrophobic transfer energies that provides a useful perspective for understanding the structural vulnerabilities of PrP^C.

Acknowledgements

References

Aronoff-Spencer, E., Burns, C.S., Avdievich, N.I., Gerfen, G.J., Peisach, J., Antholine, W.E. et al. 2000. Identification of the Cu2+ binding sites in the N-terminal domain of the prion protein by EPR and CD spectroscopy. Biochemistry **39**(45): 13760–13771.

Baker, N.A., Sept, D., Joseph, S., Holst, M.J., and McCammon, J.A. 2001. Electrostatics of nanosystems: application to microtubules and the ribosome. Proc. Natl. Acad. Sci. USA **98**(18): 10037–10041.

Bamdad, K. and Naderi-Manesh, H. 2007. Contribution of a putative salt bridge and backbone dynamics in the structural instability of human prion protein under r208h mutation. Biochem. Biophys. Res. Comm. **364**(4): 719–724.

Bas, D.C., Rogers, D. M., and Jensen, J. H. 2008. Very fast prediction and rationalization of pKa values for protein-ligand complexes. Proteins **73**(3): 765–783.

Brooks, B.R., Bruccoleri, R.E., Olafson, D.J., States, D.J., Swaminathan, S., and Karplus, M. 1983. CHARMM: A program for macromolecular energy, minimization, and dynamics calculations. J. Comp. Chem. **4**(2): 187–217.

Caughey, B., Baron, G.S., Chesebro, B., and Jeffrey, M. 2009. Getting a Grip on Prions: Oligomers, Amyloids, and Pathological Membrane Interactions. Ann. Rev. Biochem. **78**(1): 177–204.

Calzolai, L., Lysek, D. A., Perez, D. R., Guntert, P. and Wuthrich, K. 2005. Prion protein NMR structures of chickens, turtles, and frogs. Proc. Natl. Acad. Sci. U.S.A. **102**(3): 651–655.

Chiti, F., Calamai, M., Taddei, N., Stefani, M., Ramponi, G., and Dobson, C.M. 2002. Studies of the aggregation of mutant proteins in vitro provide insights into the genetics of amyloid diseases. Proc. Natl. Acad. Sci. U.S.A. **99**(4): 16419–16426.

Chiti, F., Stefani, M., Taddei, N., Ramponi, G., and Dobson, C.M. 2003. Rationalization of the effects of mutations on peptide and protein aggregation rates. Nature **424**: 805–808.

Christen, B., Hornemann, S., Damberger, F.F., and Wuthrich, K. 2009. Prion protein NMR structure from tammar wallaby (Macropus eugenii) shows that the beta2-alpha2 loop is modulated by long-range sequence effects. J. Mol. Biol. **389**(5): 833–845.

Cobb, N.J., Sonnichsen, F.D., McHaourab, H., and Surewicz, W.K. 2007. Molecular architecture of human prion protein amyloid: a parallel, in-register beta-structure. Proc. Natl. Acad. Sci. U.S.A. **104**(48): 18946–18951.

DeMarco, M. L. and Daggett, V. 2007. Molecular mechanism for low pH triggered misfolding of the human prion protein. Biochemistry **46**(11): 3045–3054.

Dima, R.I. and Thirumalai, D. 2004. Proteins associated with diseases show enhanced sequence correlation between charged residues. Bioinformatics **20**(15): 2345–2354.

Dolinsky, T.J., Nielsen, J.E., McCammon, J.A., and Baker, N.A. 2004. PDB2PQR: an automated pipeline for the setup, execution, and analysis of Poisson-Boltzmann electrostatics calculations. Nucleic Acids Res. **32**:W665-W667.

Frohlich, H. 1949. Theory of Dielectrics. Clarendon Press, London, UK.

Gossert, A. D., Bonjour, S., Lysek, D. A., Fiorito, F., and Wuthrich, K. 2005. Prion protein NMR structures of elk and of mouse/elk hybrids. Proc. Natl. Acad. Sci. U.S.A. **102**(3): 646–650.

Govaerts, C., Wille, H., Prusiner, S. B., and Cohen, F. E. 2004. Evidence for assembly of prions with left-handed beta-helices into trimers. Proc. Natl. Acad. Sci. U.S.A. **101**(22): 8342–8347.

Gu, W., Wang, T., Zhu,, J., Shi, Y., and Liu, H. 2003. Molecular dynamics simulation of the unfolding of the human prion protein domain under low pH and high temperature conditions. Biophys. Chem. **104**(1): 79–94.

Guest, W., Cashman, N.R., and Plotkin, S.S. 2009. On the inhomogeneous and anisotropic dielectric properties of proteins. Submitted to J. Am. Chem. Soc.

Hendsch, Z.H., Jonsson, T., Sauer, R.T., and Tidor, B. 1996. Protein stabilization by removal of unsatisfied polar groups: computational approaches and experimental tests. Biochemistry **35**(24): 7621–7625.

Hornemann, S. and Glockshuber, R. 1998. A scrapie-like unfolding intermediate of the prion protein domain PrP(121-231) induced by acidic pH. Proc. Natl. Acad. Sci. U.S.A. **95**(11): 6010–6014.

Kovacs, G.G., Trabattoni, G., Hainfellner, J.A., Ironside, J.W., Knight, R.S., and Budka, H. 2002. Mutations of the prion protein gene phenotypic spectrum. J. Neurol. **249**(11): 1567–1582.

Kumar, S., and Nussinov, R. 1999. Salt bridge stability in monomeric proteins. J Mol Biol **293**(5): 1241.

Langella, E., Improta, R., and Barone, V. 2004. Checking the pH-induced conformational transition of prion protein by molecular dynamics simulations: effect of protonation of histidine residues. Biophys. J. **87**(6): 3623–3632.

Li, L., Guest, W., Huang, A., Plotkin, S. S., and Cashman, N. R. 2009. Immunological mimicry of PrPC-PrPSc interactions: antibody-induced PrP misfolding. Protein Eng. Des. Sel. **22**(8): 523–529.

Liemann, S. and Glockshuber, R. 1999. Influence of amino acid substitutions related to inherited human prion diseases on the thermodynamic stability of the cellular prion protein. Biochemistry **38**(11): 3258–3267.

Liu, H., Farr-Jones, S., Ulyanov, N. B., Llinas, M., Marqusee, S., Groth, D., et al. 1999. Solution structure of Syrian hamster prion protein rPrP(90-231). Biochemistry **38**(17): 5362–5377.

Lopez Garcia, F., Zahn, R., Riek, R., and Wuthrich, K. 2000. NMR solution of the bovine prion protein. Proc. Natl. Acad. Sci. U.S.A. **97**(1): 8334–8339.

Lysek, D. A., Schorn, C., Nivon, L. G., Esteve-Moya, V., Christen, B., Calzolai, L. et al. 2005. Prion protein NMR structures of cats, dogs, pigs, and sheep. Proc. Natl. Acad. Sci. U.S.A. **102**(3): 640–645.

Ma, B., and Nussinov, R. 2002. Stabilities and conformations of Alzheimer's β-amyloid peptide oligomers (Aβ16-22, Aβ16-35, and Aβ10-35): Sequence effects. Proc. Natl. Acad. Sci. U.S.A. **99**(22): 14126–14131.

Mills, N.L., Surewicz, K., Surewicz, W.K., and Sonnichsen, F.D. 2009. NMR studies of a pathogenic mutant (D178N) of the human prion protein. To be published.

Oster, G. and Kirkwood, J.G. 1943. The influence of hindered molecular rotation on the dielectric constants of water, alcohols, and other polar liquids. J Chem Phys **11**(125): 175–178.

Paramithiotis, E., Pinard, M., Lawton, T., LaBoissiere, S., Leathers, V. L., Zou, W. Q. et al. 2003. A prion protein epitope selective for the pathologically misfolded conformation. Nat. Med. **9**: 893–899.

Polymenidou, M., Trusheim, H., Stallmach, L., Moos, R., Julius, C., Miele, G. et al. 2008. Canine MDCK cell lines are refractory to infection with human and mouse prions. Vaccine **26**(21): 2601–2614.

Prusiner, S. B. 1998. Prions. Proc. Natl. Acad. Sci. U.S.A. **95**(23): 13363–13383.

Riek, R., Hornemann, S., Wider, G., Billeter, M., Glockshuber, R., and Wuthrich, K. 1996. NMR structure of the mouse prion protein domain PrP(121-321). Nature **382**(2): 180–182.

Schmittschmitt, J.P., and Scholtz, M.J. 2003. The role of protein stability, solubility, and net charge in amyloid fibril formation. Protein Sci. **12**(10): 2374–2378.

Speare, J.O., Rush, T.S., Bloom, M.E., and Caughey, B. 2003. The role of helix 1 aspartates and salt bridges in the stability and conversion of the prion protein. J. Biol. Chem. **278**(14): 12522–12529.

Swietnicki, W., Petersen, R.B., Gambetti, P. and Surewicz, W.K. 1998. Familial mutations and the thermodynamic stability of the recombinant prion protein. J. Biol. Chem. **47**(44): 31048–31052.

Tsemekhman, K., Goldschmidt, L., Eisenberg, D., and Baker, D. 2007. Cooperative hydrogen bonding in amyloid formation. Protein Sci. **16**(4): 761–764.

Uversky, V.N., Gillespie, J.R., and Fink, A.L. 2000. Why are "natively unfolded" proteins unstructured under physiologic conditions? Proteins: Struct. Funct. Bioinf. **41**(3): 415–427.

Viles, J.H., Donne, D., Kroon, G., Prusiner, S.B., Cohen, F.E., Dyson, H.J et al. 2001. Local structural plasticity of the prion protein. Analysis of NMR relaxation dynamics. Biochemistry **40**(9): 2743–2753.

Viles, J.H., Klewpatinond, M., and Nadal, R.C. 2008. Copper and the structural biology of the prion protein. Biochem. Soc. Trans. **36**(6): 1288–1292.

Voges, D. and Karshikoff, A. 2000. A model of a local dielectric constant in proteins. J. Chem. Phys. **108**(5): 2219–2227.

Warwicker, J. 1999. Modelling charge interactions in the prion protein: predictions for pathogenesis. FEBS Letters **450**(1): 144–148.

Zahn, R., Liu, A., Luhrs, T., Riek, R., Schroetter, C., Lopez Garcia, F., et al. 2000. NMR solution structure of the human prion protein. Proc. Natl. Acad. Sci. U.S.A. **97**(1): 145–150.

Zhang, Y., Swietnicki, W., Zagorski, M.G., Surewicz, W.K., and Sonnichsen, F.D. 2000. Solution structure of the E200K variant of human prion protein. Implications for the mechanism of pathogenesis in familial prion diseases. J. Biol. Chem. **275**(43): 33650–33654.

Zuegg, J. and Gready, J.E. 1999. Molecular dynamics simulations of human prion protein: importance of correct treatment of electrostatic interactions. Biochemistry **38**(42): 13862–13876.
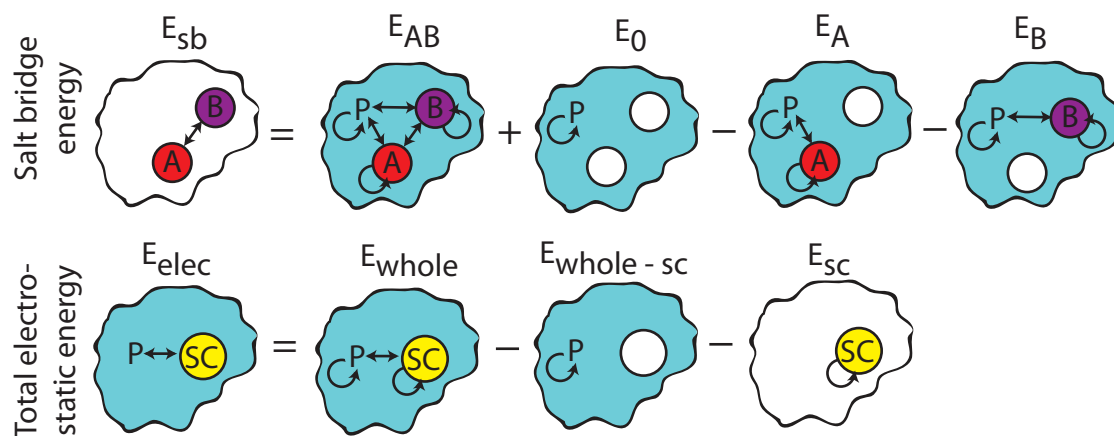
Figure 1: Schematic of the approach for calculating salt bridge and total electrostatic energies. Circular arrows denote solvation/self energies; straight arrows denote interaction energies. Labels refer to quantities in Equations 2 and 3.
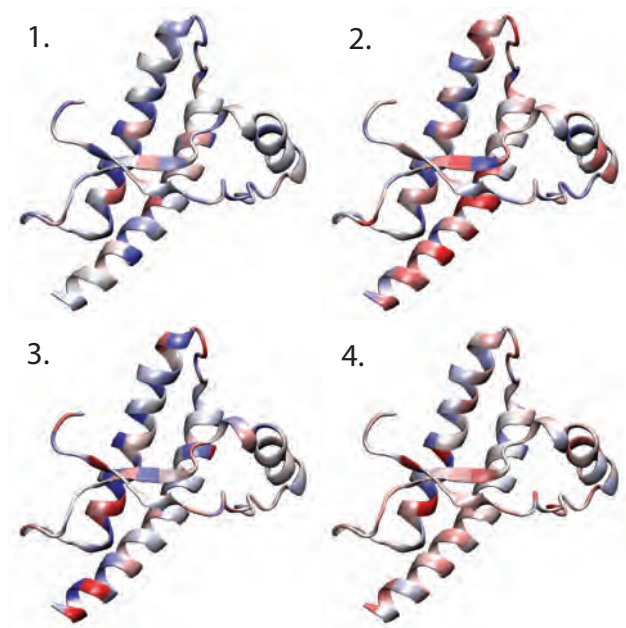
Figure 2: The 4 largest amplitude dipole correlation modes for human PrP. Regions of the same colour move in synchrony, while regions of different colours move in opposition.
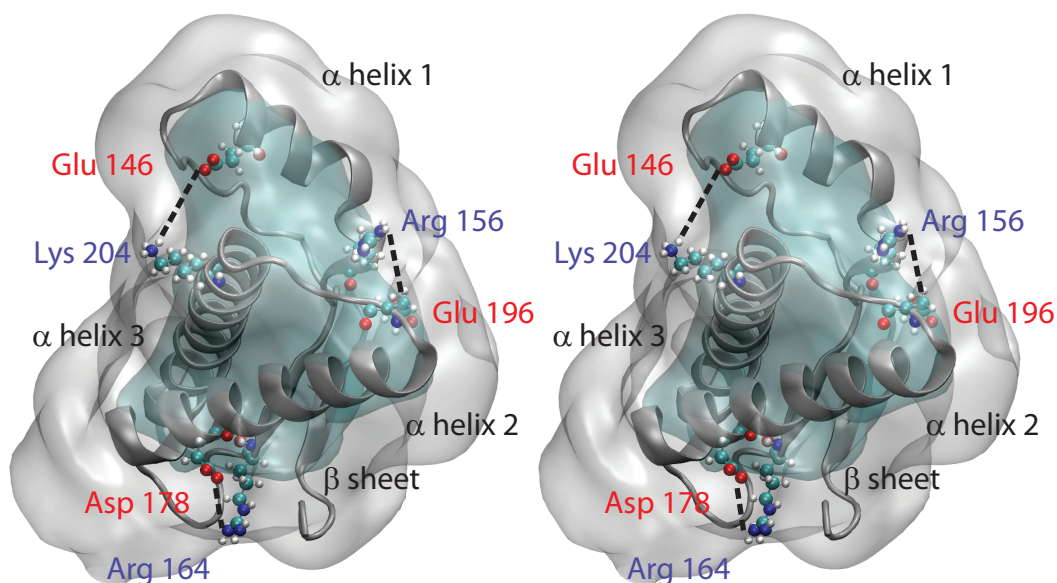
Figure 3: Stereo view of the three well-conserved nonlocal salt bridges as they are arranged in bovine PrP. The transparent surfaces show contours of equal dielectric (5 for blue; 70 for white) as determined from heterogeneous mesoscopic dielectric theory (Guest et al. 2009).The volume near the surface of the protein shows the greatest difference in dielectric on comparison of the homogeneous and heterogeneous dielectric fields. See also Figure 1 in the supplementary material for a surface plot of the dielectric permittivity as a function of position.

Frog 206 - 210 (-29.7) Wallaby 156 - 202 (-13.3) Cat 156 - 202 (-11.8) Cat 147 - 151 (-11.6) Chicken 159 - 215 (+5.2)
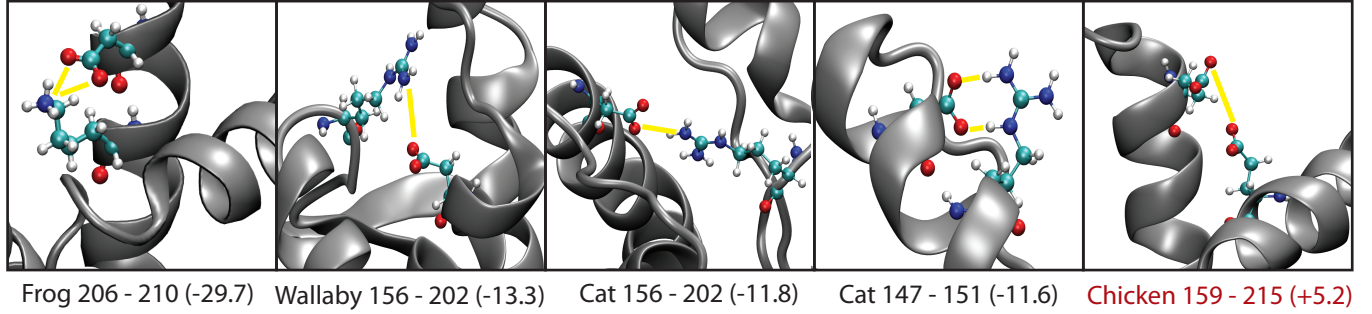
Figure 4: The 4 most attractive salt bridges (in black lettering) and the 1 most repulsive (in red lettering) identified in the set of PrP structures. Numbers in parentheses are the salt bridge energies in kJ/mol for the structures indicated. Note that interactions with all surrounding residues were considered when assessing the total effect of each residue on overall stability, as given in Table 3 and Supplementary Table 2.

					1QLX	1QLZ		1QLX	1QLZ	
	Residues Involved			r	$E_{sb}(1)$	$E_{sb}(1)$	$\frac{\delta E_{sb}(1)}{E_{sb}(1)}$	$E_{sb}(2)$	$E_{sb}(2)$	$\frac{\delta E_{sb}(2)}{E_{sb}(2)}$
				(Å)	(kJ/mol)	(kJ/mol)		(kJ/mol)	(kJ/mol)	
†HIS	140	ASP	147	6.6	-4.0	-3.7	0.30	-4.6	-4.2	0.40
ASP	144	ASP	147	7.6	2.7	4.4	0.19	2.9	5.4	0.32
GLU	146	LYS	204	7.4	-2.5	-3.0	0.29	-2.5	-3.4	0.43
ARG	148	ARG	151	7.9	1.8	2.2	1.23	1.4	2.3	0.51
ARG	148	GLU	152	4.8	-7.4	-5.0	0.25	-35.4	-14.6	0.51
ARG	156	GLU	196	4.9	-5.5	-5.1	0.32	-18.2	-11.8	0.96
ARG	156	ASP	202	7.1	-3.8	-3.0	0.27	-4.8	-3.8	0.39
ARG	164	ASP	167	6.9	-3.0	-2.4	0.54	-3.7	-2.7	0.95
ARG	164	ASP	178	6.0	-20.4	-4.8	1.23	-48.2	-8.2	1.44
†HIS	177	GLU	207	6.6	-2.8	-2.8	0.43	-2.7	-3.1	0.58
†HIS	187	ASP	202	8.0	-3.0	-3.2	0.25	-5.1	-4.6	0.30
GLU	196	ASP	202	7.9	2.9	2.4	0.22	2.9	2.7	0.25
GLU	200	LYS	204	4.1	-4.9	-3.7	0.39	-7.5	-6.5	0.85
ARG	208	GLU	211	2.6	-9.3	-5.8	0.30	-37.9	-14.9	0.66

Table 1: Salt bridges in the human prion protein from 1QLX (a single structure) and 1QLZ (an ensemble of 20 structures). †: Only present at low pH. The separation between charged groups is given by r. $E_{sb}(1)$ is the salt bridge energy (an average for 1QLZ) calculated with the heterogeneous dielectric theory, and $E_{sb}(2)$ is the same energy calculated with a constant protein dielectric of 4. The standard deviation of salt bridge energy over the structures in the NMR ensemble containing the salt bridge is given as a fraction of the total salt bridge energy by $\frac{\delta E_{sb}}{E_{sb}}$. The correlation coefficient between salt bridge energies from 1QLX and 1QLZ is 0.82.
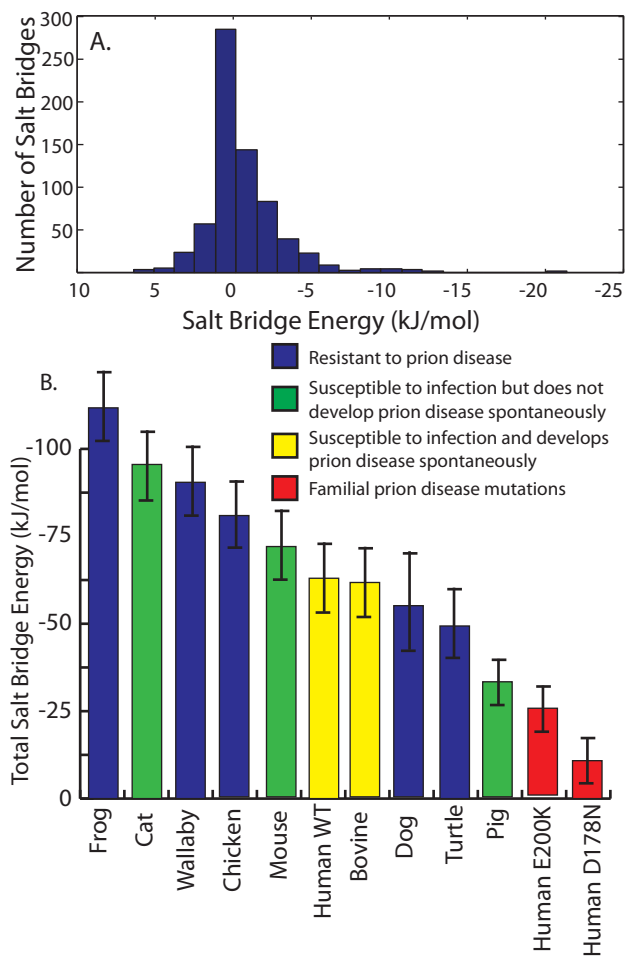
Figure 5: A. Histogram of average energies for all salt bridges identified. B. Total salt bridge energies in the molecular species studied. Error bars give the 95% confidence interval for the mean salt bridge energy from each ensemble of NMR structures.
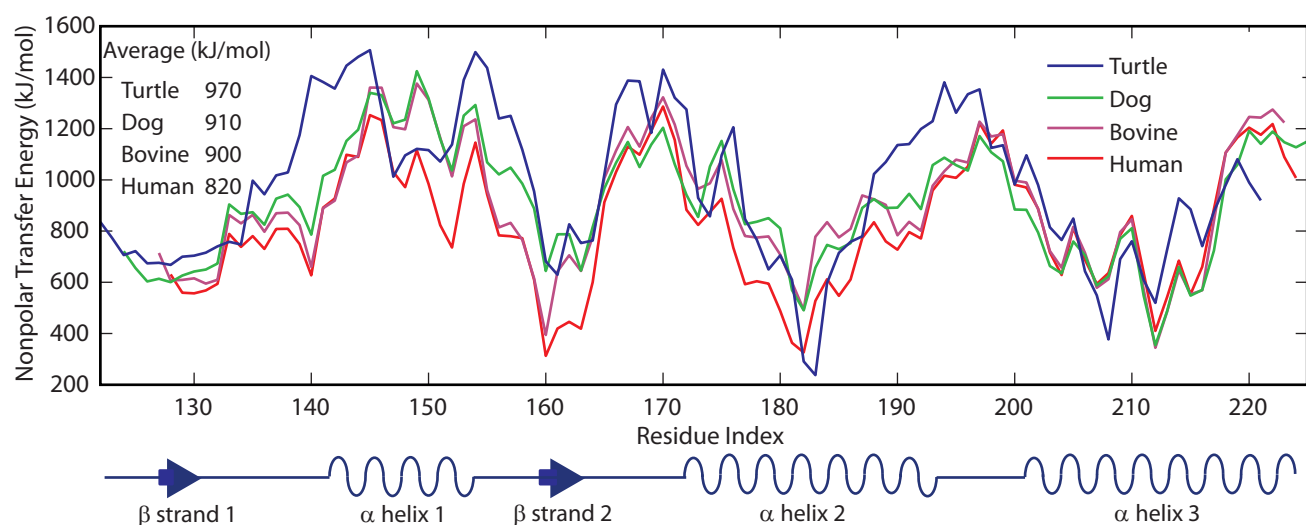
Figure 6: Hydrophobic transfer energy for strands of 7 residues centred on a given residue index as calculated from Equation 4 for 4 species of PrP^C. The numbers in the upper left hand corner give the average transfer energy over the whole protein. Shown below are the locations of secondary structural elements in the PrP^C sequence.

PDB	Species	Residues Involved				n	$E_{sb}(1)$	$\frac{\delta E_{sb}(1)}{E_{sb}(1)}$	$E_{sb}(2)$	$\frac{\delta E_{sb}(2)}{E_{sb}(2)}$
						(/20)	(kJ/mol)		(kJ/mol)	
1XU0	Frog	ASP	206	LYS	210	20	-21.4	0.31	-42.2	0.37
1QLZ	Human WT	GLU	221	ARG	228	12	-13.7	0.07	-76.6	0.07
2KFL	Wallaby	ARG	156	ASP	202	20	-13.3	0.88	-18.0	0.90
1QLZ	Human WT	ASP	167	ARG	228	11	-13.1	0.06	-75.5	0.08
1XYJ	Cat	ARG	156	ASP	202	20	-11.8	0.45	-21.5	0.69
1XYJ	Cat	ASP	147	ARG	151	20	-11.6	0.27	-40.9	0.33
2KFL	Wallaby	ARG	156	GLU	196	20	-10.9	0.32	-29.6	0.51
1XYX	Mouse	ARG	156	ASP	202	20	-10.4	0.37	-18.9	0.46
1QLZ	Human WT	ASP	147	ARG	151	20	-9.9	0.38	-30.4	0.53
1XYX	Mouse	GLU	146	LYS	204	20	-9.7	0.26	-27.2	0.44
$\vdots$	$\vdots$	$\vdots$	$\vdots$	$\vdots$	$\vdots$	$\vdots$	$\vdots$	$\vdots$	$\vdots$	$\vdots$
2K1D	Human D178N	ARG	156	LYS	194	20	3.4	0.42	4.9	0.84
1XYQ	Pig	GLU	207	GLU	211	20	3.4	0.24	4.0	0.30
1FKC	Human E200K	LYS	204	ARG	208	20	3.4	0.15	3.7	0.24
1XYQ	Pig	ARG	148	ARG	151	20	3.5	0.09	4.1	0.24
1XYX	Mouse	GLU	207	GLU	211	10	3.5	0.14	4.0	0.20
1XYK	Dog	GLU	207	GLU	211	20	4.0	0.18	4.8	0.25
1QLZ	Human WT	ASP	144	ASP	147	19	4.4	0.18	5.4	0.31
1XU0	Frog	LYS	197	LYS	210	19	4.7	0.49	7.7	0.84
2KFL	Wallaby	GLU	196	ASP	202	20	4.9	0.14	7.4	0.22
1U3M	Chicken	GLU	159	GLU	215	20	5.2	0.15	6.2	0.43

Table 2: The most attractive and repulsive salt bridges in the set of prion protein structures studied. The number of NMR conformers for each species in which the salt bridge is present is n. $E_{sb}(1)$ is the salt bridge energy (an average for 1QLZ) calculated with the heterogeneous dielectric theory, and $E_{sb}(2)$ is the same energy calculated with a constant protein dielectric of 4. The standard deviation of salt bridge energy over the structures in the NMR ensemble containing the salt bridge is given as a fraction of the total salt bridge energy by $\frac{\delta E_{sb}}{E_{sb}}$.

Res	Site	E_{elec} (kJ/mol)	$E_{elec}/$ Avg(E_{elec})
		1QLX	
THR 183	$\alpha2$	-197	6.0
ASP 147	$\alpha1$	-196	5.9
TYR 150	$\alpha1$	-171	5.2
ARG 136	$\beta1$-$\alpha1$	-151	4.6
ASP 202	$\alpha3$	-137	4.2
ARG 164	$\beta2$	-99	3.0
ASP 178	$\alpha2$	-96	2.9
GLU 221	$\alpha3$	-92	2.8
TYR 157	$\alpha1$-$\beta2$	-75	2.3
VAL 210	$\alpha3$	-73	2.2
		1QLZ	
THR 183	$\alpha2$	-171	5.9
TYR 150	$\alpha1$	-171	5.9
ASP 202	$\alpha3$	-135	4.6
TYR 157	$\alpha1$-$\beta2$	-97	3.3
ARG 164	$\beta2$	-81	2.8
THR 192	$\alpha2$-$\alpha2$	-67	2.3
ASP 178	$\alpha2$	-67	2.3
VAL 210	$\alpha3$	-65	2.2
ARG 136	$\beta1$-$\alpha1$	-63	2.1
GLU 221	$\alpha2$	-61	2.1

Table 3: Residues in human PrP (1QLX and 1QLZ) with the greatest total electrostatic energy from Equation 4. The last column gives the factor by which each residue's electrostatic energy exceeds the average for all residues in the protein (-33 kJ/mol). THR 183 has the lowest electrostatic energy in human PrP and is also a minimum on the hydrophobic transfer profile (see Figure 6), due presumably to its low dielectric local environment. VAL 210 appears in the list despite being a putatively nonpolar residue because it is located in a region of particularly low dielectric in the protein core, which increases the energy of its small side chain methyl group dipoles. $\beta1$-$\alpha1$: Between $\alpha1$ and $\beta1$. $\alpha1$-$\beta2$: Between $\alpha1$ and $\beta2$. **Bold**: Wild-type residues at the locations of known mutation sites in familial prion diseases. The correlation between transfer energies from 1QLX and 1QLZ is 0.87. With 90% confidence, the list is significantly enriched in pathologic mutations compared to random chance (p = 0.096).

Supplementary Information for

"Salt Bridges in the Prion Protein:
Implications for Stability and Misfolding"

Will Guest, Neil Cashman, and Steven Plotkin

April 12, 2010
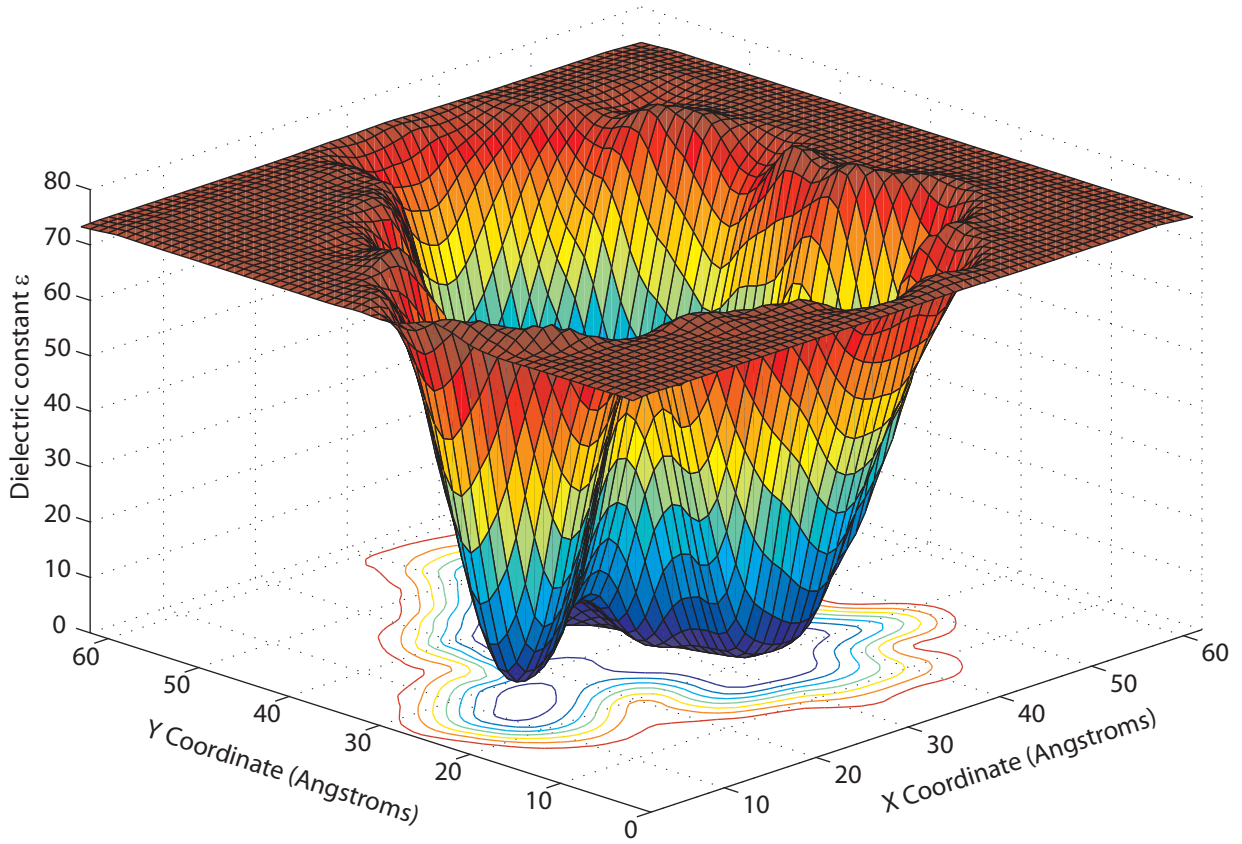
Figure 1: Local heterogeneous dielectric map of human PrP as calculated by mesoscopic dielectric theory (Guest et al., 2009). This is a slice taken through the geometric centre of the molecule in the X-Y plane.

Table 1: Salt bridges in 13 structures of the prion protein with a repulsive or attractive energy greater than 3 kJ/mol. The number of NMR conformers in which the participating charged groups are within a distance of 12Å is n. $E_{sb}(1)$ is the salt bridge energy calculated according to Equation 2 with the heterogeneous dielectric theory, and $E_{sb}(2)$ is the same energy calculated with a constant protein dielectric of 4. The standard deviation of salt bridge energy over the structures in the NMR ensemble containing the salt bridge is given by δE_{sb} and as a fraction of the total salt bridge energy by $\frac{\delta E_{sb}}{E_{sb}}$.

PDB	Species	Residues Involved		n (/20)	$E_{sb}(1)$ (kJ/mol)	$\delta E_{sb}(1)$ (kJ/mol)	$\frac{\delta E_{sb}(1)}{E_{sb}(1)}$	$E_{sb}(2)$ (kJ/mol)	$\delta E_{sb}(2)$ (kJ/mol)	$\frac{\delta E_{sb}(2)}{E_{sb}(2)}$
1DX0	Bovine	147	151	20	-6.4	3.5	0.54	-15.2	12.6	0.83
1DX0	Bovine	164	178	20	-3.1	1.9	0.60	-6.2	6.3	1.02
1DX0	Bovine	156	196	20	-6.0	2.8	0.47	-12.1	8.7	0.72
1DX0	Bovine	156	202	20	-7.8	5.5	0.71	-13.0	10.7	0.82
1DX0	Bovine	200	204	20	-3.1	1.4	0.46	-4.1	5.9	1.44
1DX0	Bovine	208	211	20	-5.1	1.9	0.38	-10.4	10.2	0.98
1FKC	Human E200K	164	167	19	-3.0	1.1	0.38	-3.2	2.0	0.64
1FKC	Human E200K	164	178	20	-4.6	1.0	0.23	-7.0	3.8	0.55
1FKC	Human E200K	156	196	20	-3.1	0.7	0.22	-3.2	1.5	0.46
1FKC	Human E200K	156	202	20	-3.2	0.7	0.21	-4.6	1.5	0.34
1FKC	Human E200K	146	204	20	-5.2	1.6	0.31	-8.6	5.1	0.59
1FKC	Human E200K	204	208	20	3.4	0.5	0.15	3.7	0.9	0.25
1FKC	Human E200K	208	211	20	-4.2	0.6	0.14	-5.2	1.8	0.33
1QLZ	Human WT	144	147	19	4.4	0.8	0.19	5.4	1.7	0.32
1QLZ	Human WT	144	151	16	-3.5	1.0	0.29	-4.1	2.5	0.60
1QLZ	Human WT	147	151	20	-9.9	3.8	0.39	-30.4	16.2	0.53
1QLZ	Human WT	148	152	19	-5.0	1.2	0.25	-14.6	7.5	0.51
1QLZ	Human WT	164	168	12	-3.3	1.7	0.53	-4.9	6.5	1.32
1QLZ	Human WT	164	178	15	-4.8	5.9	1.23	-8.2	11.8	1.44
1QLZ	Human WT	156	196	20	-5.1	1.6	0.32	-11.8	11.4	0.96
1QLZ	Human WT	146	204	18	-3.0	0.9	0.29	-3.4	1.4	0.43
1QLZ	Human WT	200	204	20	-3.7	1.5	0.39	-6.5	5.5	0.85
1QLZ	Human WT	204	207	15	-3.1	1.4	0.45	-3.7	5.9	1.58
1QLZ	Human WT	208	211	20	-5.8	1.8	0.30	-14.9	9.9	0.66
1QLZ	Human WT	167	228	11	-13.1	0.9	0.07	-75.5	5.7	0.07
1QLZ	Human WT	221	228	12	-13.7	1.0	0.07	-76.6	5.7	0.07
1U3M	Chicken	150	153	20	-5.0	1.3	0.25	-10.1	7.3	0.72
1U3M	Chicken	155	159	20	-3.8	0.7	0.19	-5.2	2.3	0.43
1U3M	Chicken	171	185	20	-5.4	1.6	0.29	-12.4	6.7	0.54
1U3M	Chicken	159	215	20	5.2	0.8	0.15	6.2	2.7	0.44
1U3M	Chicken	163	219	20	-8.4	4.3	0.51	-20.6	15.9	0.77
1U3M	Chicken	217	221	20	-5.7	1.1	0.20	-15.3	7.6	0.50
1U3M	Chicken	225	229	20	-4.1	1.8	0.44	-5.9	7.7	1.30
1U3M	Chicken	139	237	20	-4.1	2.0	0.48	-6.0	6.0	0.99
1U5L	Turtle	143	146	20	-3.3	0.7	0.21	-5.8	2.3	0.40
1U5L	Turtle	165	169	18	-3.0	2.2	0.74	-5.0	7.1	1.42
1U5L	Turtle	164	179	20	-5.1	2.8	0.55	-7.9	7.9	1.00
1U5L	Turtle	175	179	20	-4.2	2.8	0.68	-6.9	7.3	1.06

Continued...

2

PDB	Species	Residues Involved		n (/20)	$E_{sb}(1)$ (kJ/mol)	$\delta E_{sb}(1)$ (kJ/mol)	$\frac{\delta E_{sb}(1)}{E_{sb}(1)}$	$E_{sb}(2)$ (kJ/mol)	$\delta E_{sb}(2)$ (kJ/mol)	$\frac{\delta E_{sb}(2)}{E_{sb}(2)}$
1U5L	Turtle	156	202	16	-3.1	2.5	0.79	-4.2	6.8	1.63
1U5L	Turtle	146	204	20	-5.7	1.8	0.32	-15.1	10.8	0.71
1U5L	Turtle	191	207	20	-4.6	2.6	0.56	-7.5	8.7	1.15
1XU0	Frog	148	152	20	-3.3	1.3	0.39	-4.7	6.2	1.31
1XU0	Frog	169	176	19	-3.1	1.6	0.52	-5.6	6.6	1.17
1XU0	Frog	175	179	20	-3.1	1.3	0.43	-4.8	7.0	1.45
1XU0	Frog	169	180	19	3.0	1.4	0.46	4.1	2.8	0.69
1XU0	Frog	188	192	20	-9.4	1.8	0.19	-19.3	6.3	0.33
1XU0	Frog	197	206	20	-5.3	3.4	0.63	-10.2	11.9	1.16
1XU0	Frog	197	210	19	4.7	2.3	0.50	7.7	6.5	0.85
1XU0	Frog	206	210	20	-21.4	6.7	0.32	-42.2	15.9	0.38
1XU0	Frog	163	221	20	-9.4	6.1	0.64	-16.9	13.6	0.80
1XU0	Frog	221	224	20	-5.0	3.6	0.72	-11.5	12.1	1.05
1XYJ	Cat	147	151	20	-11.6	3.1	0.27	-40.9	13.4	0.33
1XYJ	Cat	164	178	20	-4.7	2.5	0.54	-11.7	11.9	1.01
1XYJ	Cat	156	202	20	-11.8	5.3	0.44	-21.5	15.0	0.70
1XYJ	Cat	146	204	20	-3.9	2.0	0.51	-5.7	8.7	1.51
1XYJ	Cat	200	204	20	-3.5	0.9	0.26	-4.0	3.4	0.85
1XYJ	Cat	208	211	20	-5.8	3.0	0.52	-11.8	11.3	0.96
1XYK	Dog	144	147	20	3.1	1.0	0.32	3.9	2.0	0.52
1XYK	Dog	144	148	20	-4.1	2.1	0.51	-9.3	9.1	0.97
1XYK	Dog	147	151	20	-8.4	4.5	0.54	-22.5	16.5	0.73
1XYK	Dog	148	152	20	-3.1	1.2	0.39	-5.3	5.8	1.09
1XYK	Dog	164	178	20	-3.6	2.2	0.60	-7.4	9.3	1.25
1XYK	Dog	136	202	2	-4.0	0.8	0.19	-6.1	0.8	0.12
1XYK	Dog	200	204	20	-3.1	1.2	0.40	-3.8	4.7	1.22
1XYK	Dog	204	207	20	-3.8	1.4	0.38	-5.6	6.2	1.11
1XYK	Dog	207	211	20	4.0	0.7	0.16	4.8	1.2	0.26
1XYK	Dog	208	211	20	-5.3	2.5	0.48	-11.5	11.3	0.98
1XYQ	Pig	147	151	20	-4.3	1.3	0.29	-6.0	4.1	0.69
1XYQ	Pig	148	151	20	3.5	0.3	0.09	4.1	1.0	0.24
1XYQ	Pig	164	178	20	-5.9	1.5	0.25	-11.9	7.0	0.59
1XYQ	Pig	200	204	20	-4.0	1.3	0.33	-7.0	6.4	0.91
1XYQ	Pig	204	207	20	-3.3	1.2	0.37	-3.0	2.1	0.71
1XYQ	Pig	207	211	20	3.4	0.8	0.23	4.0	1.2	0.30
1XYQ	Pig	208	211	20	-5.9	2.5	0.42	-9.8	12.1	1.24
1XYQ	Pig	220	223	19	-3.8	1.2	0.33	-3.6	2.4	0.67
1XYX	Mouse	144	147	12	3.2	0.8	0.25	3.2	1.3	0.41
1XYX	Mouse	147	151	16	-5.1	2.0	0.38	-9.2	7.9	0.85
1XYX	Mouse	148	152	12	-3.8	1.7	0.44	-7.8	9.3	1.18
1XYX	Mouse	164	178	18	-5.4	2.4	0.45	-10.8	11.0	1.02
1XYX	Mouse	156	196	13	-3.7	1.0	0.28	-4.2	2.5	0.61
1XYX	Mouse	194	196	16	-3.5	0.7	0.21	-3.0	0.7	0.23
1XYX	Mouse	156	202	20	-10.4	3.9	0.37	-18.9	8.8	0.46
1XYX	Mouse	146	204	20	-9.7	2.5	0.26	-27.2	11.9	0.44
1XYX	Mouse	146	208	10	-3.2	0.3	0.10	-3.8	0.9	0.23
1XYX	Mouse	204	208	18	3.2	0.4	0.13	3.6	0.9	0.24
1XYX	Mouse	207	211	10	3.5	0.5	0.15	4.0	0.8	0.20

Continued...

3

PDB	Species	Residues Involved		n (/20)	$E_{sb}(1)$ (kJ/mol)	$\delta E_{sb}(1)$ (kJ/mol)	$\frac{\delta E_{sb}(1)}{E_{sb}(1)}$	$E_{sb}(2)$ (kJ/mol)	$\delta E_{sb}(2)$ (kJ/mol)	$\frac{\delta E_{sb}(2)}{E_{sb}(2)}$
1XYX	Mouse	208	211	10	-4.4	1.1	0.24	-6.2	5.8	0.94
1XYX	Mouse	167	221	2	4.5	0.1	0.03	5.7	0.8	0.14
1XYX	Mouse	227	230	10	-3.7	1.9	0.51	-6.9	7.9	1.15
2K1D	Human D178N	144	147	20	3.3	0.4	0.13	3.6	0.9	0.23
2K1D	Human D178N	147	151	20	-3.7	1.1	0.30	-5.1	3.2	0.63
2K1D	Human D178N	164	185	19	3.3	1.5	0.45	3.7	2.8	0.78
2K1D	Human D178N	156	194	20	3.4	1.4	0.40	4.9	4.1	0.85
2K1D	Human D178N	156	202	16	-3.5	1.9	0.53	-5.5	5.1	0.93
2K1D	Human D178N	208	211	19	-3.6	1.2	0.32	-3.0	1.4	0.46
2KFL	Wallaby	147	151	20	-5.4	2.7	0.51	-14.6	11.3	0.77
2KFL	Wallaby	148	152	20	-3.6	1.4	0.40	-7.9	7.6	0.96
2KFL	Wallaby	164	178	20	-4.8	1.9	0.39	-8.3	7.8	0.93
2KFL	Wallaby	178	185	19	-3.3	0.9	0.27	-3.7	1.6	0.42
2KFL	Wallaby	156	196	20	-10.9	3.5	0.32	-29.6	15.1	0.51
2KFL	Wallaby	156	202	20	-13.3	11.7	0.88	-18.0	16.2	0.90
2KFL	Wallaby	196	202	20	4.9	0.7	0.13	7.4	1.6	0.22
2KFL	Wallaby	200	204	20	-4.6	1.1	0.24	-7.4	5.5	0.74
2KFL	Wallaby	204	207	20	-4.2	0.7	0.17	-4.4	1.2	0.28
2KFL	Wallaby	146	208	20	-3.7	0.3	0.09	-4.6	0.9	0.20
2KFL	Wallaby	208	211	20	-3.8	0.9	0.25	-4.8	5.0	1.04
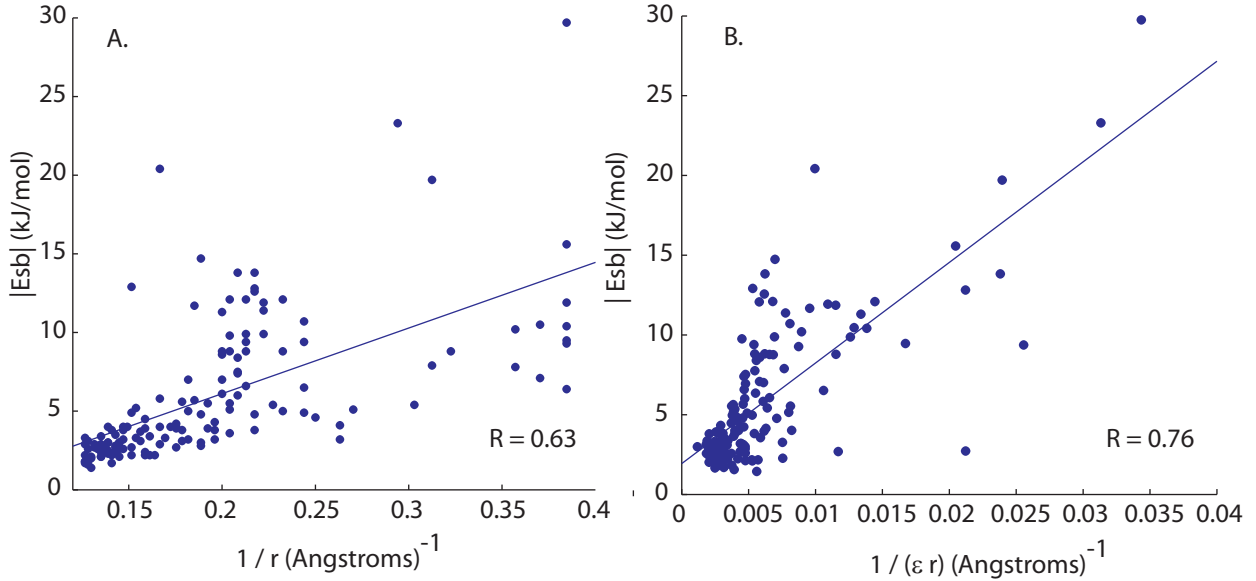
Figure 2: A. Absolute salt bridge energies as a function of the reciprocal of the separation distance between the participating charged groups. B. Absolute salt bridge energies as a function of the reciprocal of the separation distance multiplied by the dielectric constant ϵ at the midpoint of the line joining the charged groups. In a homogeneous dielectric environment, the energy of a salt bridge connecting charges q_A and q_B would be given by $E_{sb} = \frac{1}{4\pi\epsilon_0} \frac{q_A q_B}{\epsilon r}$. Including $1/\epsilon$ in the fit in addition to $1/r$ improves the correlation from 0.63 to 0.76, but even taken together the quantities ϵ and r do not reliably predict salt bridge energies. Thus a direct calculation of energies from the full heterogeneous dielectric map is necessary to obtain accurate results.

Table 2: Total electrostatic energies in kJ/mol for every residue in a selection of 13 prion protein structures at pH 7. The energies are calculated according to Equation 3.

Res	2KFL Wallaby		1QLX Human WT		1FKC Human E200K		2K1D Human D178N		1DX0 Bovine		1U3M Chicken		1U5L Turtle		1XU0 Frog		1XYJ Cat		1XYK Dog		1XYQ Pig		1XYX Mouse		1AG2 Mouse	
120	S	-11											S	-7												
121	V	-9											V	-2												
122	V	-2											V	-4			V	-4	V	-2	V	-4	V	-3		
123	G	-1											G	0			G	-1	G	-1	G	-1	G	-1		
124	G	-1											G	0			G	-1	G	-1	G	-1	G	-1		
125	L	-19							L	-7			L	-7			L	-15	L	-5	L	-8	L	-23	L	-6
126	G	-1	G	-1	G	-1	G	-1	G	-1			G	0	G	-2	G	-1	G	-1	G	-1	G	-1	G	-1
127	G	-1	G	-1	G	-1	G	-2	G	0	S	-7	G	0	G	-2	G	0	G	-1	G	0	G	-1	G	-1
128	Y	-42	Y	-32	Y	-28	Y	-18	Y	-52	V	-2	Y	-23	Y	-18	Y	-21	Y	-18	Y	-27	Y	-28	Y	-27
129	M	-11	M	-9	M	-8	V	-6	M	-7	V	-2	A	-2	M	-8	M	-7	M	-5	M	-4	M	-9	M	-8
130	L	-15	L	-10	L	-10	L	-4	L	-12	G	-1	L	-9	L	-11	L	-14	L	-7	L	-7	L	-5	L	-14
131	G	-2	G	-5	G	-5	G	-1	G	-2	G	0	G	-2	G	-3	G	-2	G	-1	G	0	G	-3	G	-4
132	S	-21	S	-18	S	-16	S	-7	S	-11	L	-3	S	-11	N	-34	S	-9	S	-14	S	-8	S	-12	S	-13
133	A	-1	A	-3	A	-1	A	-1	A	-1	G	0	A	-2	A	-2	A	-1	A	-1	A	-1	A	-3	A	-3
134	M	-8	M	-6	M	-24	M	-9	M	-30	G	0	M	-10	V	-19	M	-11	M	-6	M	-8	M	-8	M	-22
135	S	-8	S	-8	S	-14	S	-9	S	-15	Y	-10	S	-16	G	-1	S	-38	S	-19	S	-10	S	-9	S	-11
136	R	-382	R	-151	R	-140	R	-55	R	-63	A	-3	G	-1	R	-55	R	-44	R	-46	R	-56	R	-22	R	-119
137	P	-8	P	-10	P	-15	P	-4	P	-7	M	-7	M	-16	M	-22	P	-15	P	-6	P	-12	P	-15	P	-8
138	V	-6	I	-11	I	-10	I	-5	L	-7	G	-3	R	-35	S	-15	L	-4	L	-22	L	-5	M	-3	M	-4
139	M	-15	I	-20	I	-18	I	-37	I	-43	R	-59	M	-7	Y	-16	I	-18	I	-9	I	-20	I	-16	I	-26
140	H	-23	H	-25	H	-27	H	-20	H	-20	V	-13	N	-14	Q	-13	H	-12	H	-15	H	-25	H	-16	H	-15
141	F	-29	F	-18	F	-47	F	-24	F	-32	M	-13	F	-23	F	-24	F	-23	F	-20	F	-27	F	-27	F	-19
142	G	1	G	1	G	-1	G	0	G	0	S	-16	D	-26	N	-15	G	0	G	0	G	0	G	0	G	0
143	N	-17	S	-9	S	-19	S	-10	S	-26	G	-1	R	-32	N	-27	N	-33	N	-14	S	-10	N	-12	N	-15
144	E	-46	D	-36	D	-39	D	-40	D	-36	M	-10	P	-4	P	-3	D	-37	D	-40	D	-37	D	-37	D	-45
145	Y	-13	Y	-11	Y	-12	Y	-10	Y	-11	N	-11	E	-29	M	-6	Y	-12	Y	-19	Y	-10	W	-19	W	-18
146	E	-40	E	-39	E	-80	E	-43	E	-78	Y	-40	E	-90	E	-127	E	-54	E	-70	E	-43	E	-51	E	-45
147	D	-75	D	-196	D	-70	D	-61	D	-91	H	-14	R	-76	S	-31	D	-57	D	-53	D	-92	D	-54	D	-86
148	R	-54	R	-34	R	-48	R	-59	R	-34	F	-12	Q	-26	R	-50	R	-36	R	-25	R	-48	R	-40	R	-70
149	Y	-52	Y	-20	Y	-42	Y	-23	Y	-27	D	-32	W	-57	Y	-77	Y	-25	Y	-31	Y	-19	Y	-52	Y	-106
150	Y	-86	Y	-171	Y	-132	Y	-68	Y	-143	R	-42	W	-81	Y	-58	Y	-49	Y	-58	Y	-79	Y	-52	Y	-114
151	R	-97	R	-43	R	-55	R	-43	R	-69	P	-2	N	-47	N	-57	R	-51	R	-37	R	-61	R	-36	R	-46
152	E	-39	E	-31	E	-39	E	-57	E	-31	D	-33	E	-45	D	-73	E	-37	E	-42	E	-67	E	-50	E	-78
153	N	-53	N	-25	N	-49	N	-31	N	-30	E	-33	N	-36	Y	-23	N	-28	N	-85	N	-41	N	-74	N	-158
154	Q	-25	M	-24	M	-16	M	-4	M	-8	Y	-17	S	-10	Y	-16	M	-8	M	-5	M	-13	M	-10	M	-13
155	Y	-17	H	-19	H	-27	H	-19	H	-18	R	-41	N	-15	N	-13	Y	-13	Y	-9	Y	-13	Y	-13	Y	-21
156	R	-128	R	-29	R	-41	R	-60	R	-97	W	-36	R	-77	Q	-14	R	-53	R	-68	R	-57	R	-133	R	-242
157	Y	-145	Y	-75	Y	-148	Y	-18	Y	-140	W	-52	Y	-9	M	-41	Y	-109	Y	-66	Y	-52	Y	-128	Y	-228
158	P	-16	P	-12	P	-9	P	-6	P	-37	S	-13	P	-3	P	-32	P	-9	P	-4	P	-5	P	-10	P	-12
159	N	-21	N	-32	N	-52	N	-14	N	-38	E	-54	N	-59	N	-17	N	-17	D	-54	N	-16	N	-17	N	-22
160	Q	-23	Q	-34	Q	-18	Q	-24	Q	-16	N	-56	Q	-27	Q	-80	Q	-26	Q	-23	Q	-34	Q	-26	Q	-24
161	V	-63	V	-53	V	-64	V	-26	V	-54	S	-20	V	-34	V	-61	V	-50	V	-27	V	-43	V	-51	V	-49
162	M	-19	Y	-25	Y	-25	Y	-34	Y	-32	A	-1	Y	-29	Y	-38	Y	-32	Y	-34	Y	-21	Y	-40	Y	-50
163	Y	-59	Y	-51	Y	-40	Y	-31	Y	-39	R	-30	Y	-42	R	-83	Y	-45	Y	-26	Y	-23	Y	-36	Y	-30
164	R	-59	R	-99	R	-63	R	-62	R	-74	Y	-15	K	-30	P	-28	R	-52	R	-82	R	-84	R	-56	R	-182
165	P	-16	P	-5	P	-5	P	-8	P	-5	P	-5	E	-47	M	-7	P	-3	P	-3	P	-3	P	-5	P	-4
166	I	-25	M	-19	M	-21	M	-2	V	-13	N	-48	Y	-152	Y	-33	V	-15	V	-7	V	-24	V	-16	V	-34
167	D	-34	D	-41	D	-58	D	-48	D	-31	R	-67	N	-12	R	-35	D	-38	D	-54	D	-32	D	-39	D	-39
168	Q	-20	E	-31	E	-39	E	-70	Q	-11	V	-47	D	-34	G	-1	Q	-18	Q	-16	Q	-17	Q	-15	Q	-20
169	Y	-137	Y	-16	Y	-8	Y	-7	Y	-8	Y	-31	R	-48	R	-93	Y	-6	Y	-6	Y	-15	Y	-40	S	-10
170	G	-1	S	-25	S	-27	S	-9	S	-18	Y	-52	S	-10	E	-41	S	-28	S	-25	S	-8	S	-13	S	-10
171	S	-12	N	-20	N	-17	N	-13	N	-19	R	-36	V	-22	Y	-10	N	-15	N	-28	N	-18	N	-13	N	-13
172	Q	-22	Q	-11	Q	-21	Q	-15	Q	-30	D	-29	P	-3	P	-17	Q	-15	Q	-15	Q	-24	Q	-12	Q	-70
173	N	-15	N	-11	N	-16	N	-13	N	-18	Y	-131	E	-36	S	-14	N	-10	N	-13	N	-17	N	-13	N	-17
174	S	-14	N	-12	N	-14	N	-17	N	-15	S	-7	G	-1	E	-49	N	-11	N	-11	S	-11	N	-13	N	-34

Res	2KFL Wallaby		1QLX Human WT		1FKC Human E200K		2K1D Human D178N		1DX0 Bovine		1U3M Chicken		1U5L Turtle		1XU0 Frog		1XYJ Cat		1XYK Dog		1XYQ Pig		1XYX Mouse		1AG2 Mouse	
175	F	-79	F	-53	F	-54	F	-28	F	-45	S	-12	R	-134	D	-36	F	-30	F	-18	F	-73	F	-24	F	-79
176	V	-18	V	-9	V	-19	V	-19	V	-14	P	-3	F	-68	R	-47	R	-6	V	-14	V	-46	V	-10	V	-10
177	H	-17	H	-17	H	-16	H	-16	H	-18	V	-4	V	-9	F	-56	H	-14	R	-29	H	-15	H	-11	H	-17
178	D	-69	D	-96	D	-63	N	-32	D	-56	P	-3	R	-39	V	-10	D	-42	D	-52	D	-39	D	-41	D	-78
179	C	-14	C	-15	C	-12	C	-11	C	-13	Q	-24	D	-127	R	-46	C	-6	C	-8	C	-11	C	-9	C	-16
180	V	-22	V	-11	V	-12	V	-18	V	-9	D	-31	C	-13	D	-60	V	-16	V	-15	V	-38	V	-9	V	-6
181	N	-19	N	-14	N	-18	N	-17	N	-14	V	-3	V	-21	C	-11	N	-13	N	-20	N	-24	N	-9	N	-19
182	I	-30	I	-29	I	-14	I	-31	I	-18	F	-60	N	-19	Y	-13	I	-26	I	-9	I	-26	I	-10	I	-31
183	T	-212	T	-197	T	-172	T	-158	T	-193	V	-20	I	-36	N	-18	T	-166	T	-157	T	-165	T	-174	T	-219
184	V	-14	I	-34	I	-37	I	-22	V	-14	A	-1	T	-178	M	-15	V	-41	V	-8	V	-48	I	-12	I	-10
185	K	-21	K	-19	K	-23	K	-29	K	-23	D	-37	V	-31	S	-133	R	-50	K	-16	K	-21	K	-18	K	-18
186	Q	-51	Q	-23	Q	-26	Q	-20	E	-88	C	-13	T	-19	V	-9	Q	-20	Q	-58	Q	-24	Q	-28	Q	-33
187	H	-29	H	-37	H	-43	H	-34	H	-41	F	-22	E	-59	T	-26	H	-26	H	-76	H	-19	H	-50	H	-39
188	T	-29	T	-22	T	-34	T	-56	T	-34	N	-15	Y	-20	E	-84	T	-66	T	-11	T	-56	T	-18	T	-24
189	T	-21	V	-4	V	-6	V	-4	V	-4	I	-14	K	-13	Y	-107	V	-7	V	-3	V	-8	V	-3	V	-4
190	T	-16	T	-18	T	-11	T	-12	T	-26	T	-133	I	-29	I	-13	T	-18	T	-17	T	-26	T	-15	T	-28
191	T	-19	T	-23	T	-19	T	-73	T	-99	V	-20	D	-149	I	-8	I	-22	T	-31	T	-51	T	-54	T	-26
192	T	-49	T	-51	T	-50	T	-33	T	-16	T	-18	P	-4	K	-21	T	-27	T	-8	T	-20	T	-19	T	-26
193	T	-11	T	-17	T	-21	T	-8	T	-16	E	-43	N	-15	P	-4	T	-13	T	-8	T	-13	T	-10	T	-15
194	K	-16	K	-19	K	-15	K	-16	K	-20	Y	-43	E	-50	A	-2	K	-14	K	-25	K	-19	K	-18	K	-16
195	G	0	G	0	G	0	G	0	G	0	S	-8	N	-36	E	-29	G	0	G	0	G	0	G	0	G	-1
196	E	-53	E	-30	E	-41	E	-37	E	-48	I	-14	Q	-13	G	0	E	-83	E	-67	E	-46	E	-40	E	-78
197	N	-22	N	-12	N	-18	N	-18	N	-13	G	-1	N	-13	K	-19	N	-13	N	-13	N	-11	N	-19	N	-18
198	F	-34	F	-10	F	-34	F	-11	F	-42	P	-2	V	-19	N	-17	F	-24	F	-21	F	-16	F	-35	F	-23
199	T	-37	T	-29	T	-55	T	-32	T	-16	A	-2	T	-14	N	-22	T	-17	T	-34	T	-16	T	-30	T	-63
200	E	-35	E	-37	K	-17	E	-33	E	-30	A	-1	Q	-17	S	-8	E	-31	E	-31	E	-33	E	-36	E	-33
201	T	-34	T	-20	T	-25	T	-20	T	-14	K	-9	V	-6	E	-27	T	-14	T	-25	T	-13	T	-23	T	-25
202	D	-304	D	-137	D	-290	D	-122	D	-235	K	-14	E	-104			D	-123	D	-340	D	-86	D	-161	D	-372
203	I	-9	V	-5	V	-5	V	-8	I	-7	N	-14	V	-18	N	-16	M	-8	M	-5	V	-7	V	-6	V	-7
204	K	-12	K	-9	K	-12	K	-8	K	-7	K	-14	R	-46	Q	-15	K	-15	K	-11	K	-13	K	-12	K	-11
205	I	-58	M	-20	M	-40	M	-13	M	-42	S	-10	V	-74	L	-14	I	-39	I	-70	M	-15	M	-40	M	-18
206	M	-49	M	-37	M	-46	M	-17	M	-39	E	-27	M	-28	D	-119	M	-24	M	-34	I	-42	M	-47	M	-32
207	E	-61	E	-44	E	-36	E	-60	E	-42	A	-2	K	-23	T	-14	E	-51	E	-36	E	-69	E	-39	E	-45
208	R	-35	R	-35	R	-32	R	-73	R	-41	V	-4	Q	-16	T	-13	R	-58	R	-30	R	-45	R	-32	R	-27
209	V	-86	V	-66	V	-58	V	-30	V	-56	A	-1	V	-60	V	-51	V	-50	V	-41	V	-84	V	-47	V	-63
210	V	-80	V	-73	V	-73	V	-55	V	-75	A	-3	I	-81	K	-95	V	-67	V	-61	V	-82	V	-66	V	-86
211	E	-52	E	-41	E	-42	E	-59	E	-44	N	-18	Q	-16	S	-11	E	-53	E	-47	E	-94	E	-37	E	-56
212	Q	-24	Q	-17	Q	-21	Q	-104	Q	-20	Q	-13	E	-46	Q	-19	Q	-33	Q	-23	Q	-25	Q	-14	Q	-23
213	M	-31	M	-27	M	-38	M	-30	M	-41	Q	-13	M	-31	I	-82	M	-36	M	-26	M	-35	M	-36	M	-38
214	C	-14	C	-12	C	-16	C	-13	C	-14	T	-12	C	-12	C	-54	C	-8	C	-12	C	-11	C	-7	C	-19
215	I	-7	I	-7	I	-17	I	-28	I	-10	E	-44	M	-5	R	-40	V	-10	V	-7	I	-24	T	-5	V	-33
216	T	-17	T	-24	T	-57	T	-51	T	-20	V	-9	Q	-29	E	-50	T	-23	T	-24	T	-30	T	-28	T	-50
217	Q	-66	Q	-53	Q	-82	Q	-21	Q	-54	E	-25	Q	-36	M	-52	Q	-43	Q	-53	Q	-60	Q	-45	Q	-46
218	Y	-34	Y	-23	Y	-51	Y	-91	Y	-22	M	-3	Y	-22	C	-14	Y	-40	Y	-37	Y	-48	Y	-22	Y	-122
219	Q	-17	E	-37	E	-44	E	-26	Q	-15	E	-55	Q	-28	I	-10	Q	-19	Q	-17	Q	-27	Q	-15	Q	-32
220	N	-25	R	-53	R	-77	R	-33	R	-56	N	-13	Q	-18	T	-23	K	-16	K	-15	K	-16	K	-20	K	-16
221	E	-220	E	-37	E	-92	E	-77	E	-91	K	-9	Y	-33	E	-196	E	-42	E	-43	E	-58	E	-53	E	-43
222	Y	-18	S	-19	S	-40	S	-14	S	-11	N	-29	Q	-56	Y	-64	E	-52	S	-25	Y	-16	S	-29	S	-43
223	Q	-22	Q	-15	Q	-17	Q	-13	Q	-17	V	-19	L	-8	R	-41	E	-39	E	-43	E	-79	Q	-13	Q	-16
224	A	-2	A	-2	A	-2	A	-2	A	-3	T	-24	A	-2	A	-63	A	-2	A	-1	A	-2	A	-2	A	-2
225	Q	-21	Y	-16	Y	-26	Y	-17	Y	-21	K	-15			G	0	Y	-11	Y	-11	Y	-11	Y	-11	Y	-15
226	R	-46	Y	-9	Y	-22	Y	-9	Y	-13	K	-16					Y	-11	A	-1	Y	-11	Y	-11		
227	Y	-9	Q	-14	Q	-24	Q	-14			I	-56					Q	-18	Q	-22	Q	-13	D	-29		
228	R	-9			R	-41	R	-30			R	-47					R	-28	R	-33	R	-37	G	0		
229	Y	-11			G	0	G	0			E	-47					R	-29	G	1	A	-1	R	-1		
230					S	-8	S	-9			M	-41					A	-1	A	-1	A	-1	A	-1		
231											C	-9											S	-8		
232											V	-12														
233											Q	-22														
234											Q	-67														
235											Y	-41														

Continued...

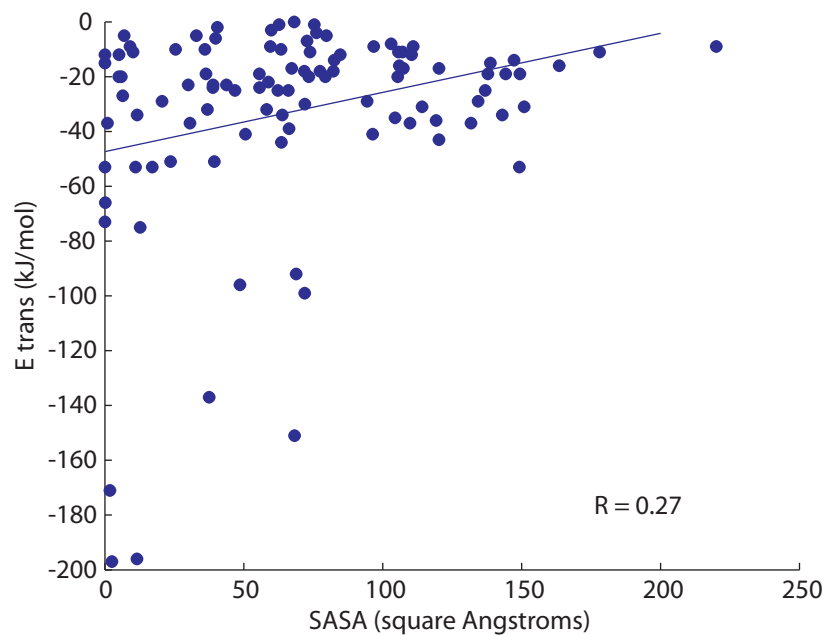| Res	2KFL Wallaby	1QLX Human WT	1FKC Human E200K	2K1D Human D178N	1DX0 Bovine	1U3M Chicken	1U5L Turtle	1XU0 Frog	1XYJ Cat	1XYK Dog	1XYQ Pig	1XYX Mouse	1AG2 Mouse
236						R -35							
237						E -55							
238						Y -22							
239						R -36							
240						L -3							
241						A -1							

Figure 3: Total electrostatic energies of side chains in human PrP calculated from Equation 3 plotted as a function of solvent-accessible surface area (SASA), a statistic related to burial in the core of the protein. There is a weak but significant (p = 0.01) correlation between the energy and SASA, but SASA alone is a poor proxy for the electrostatic energy.
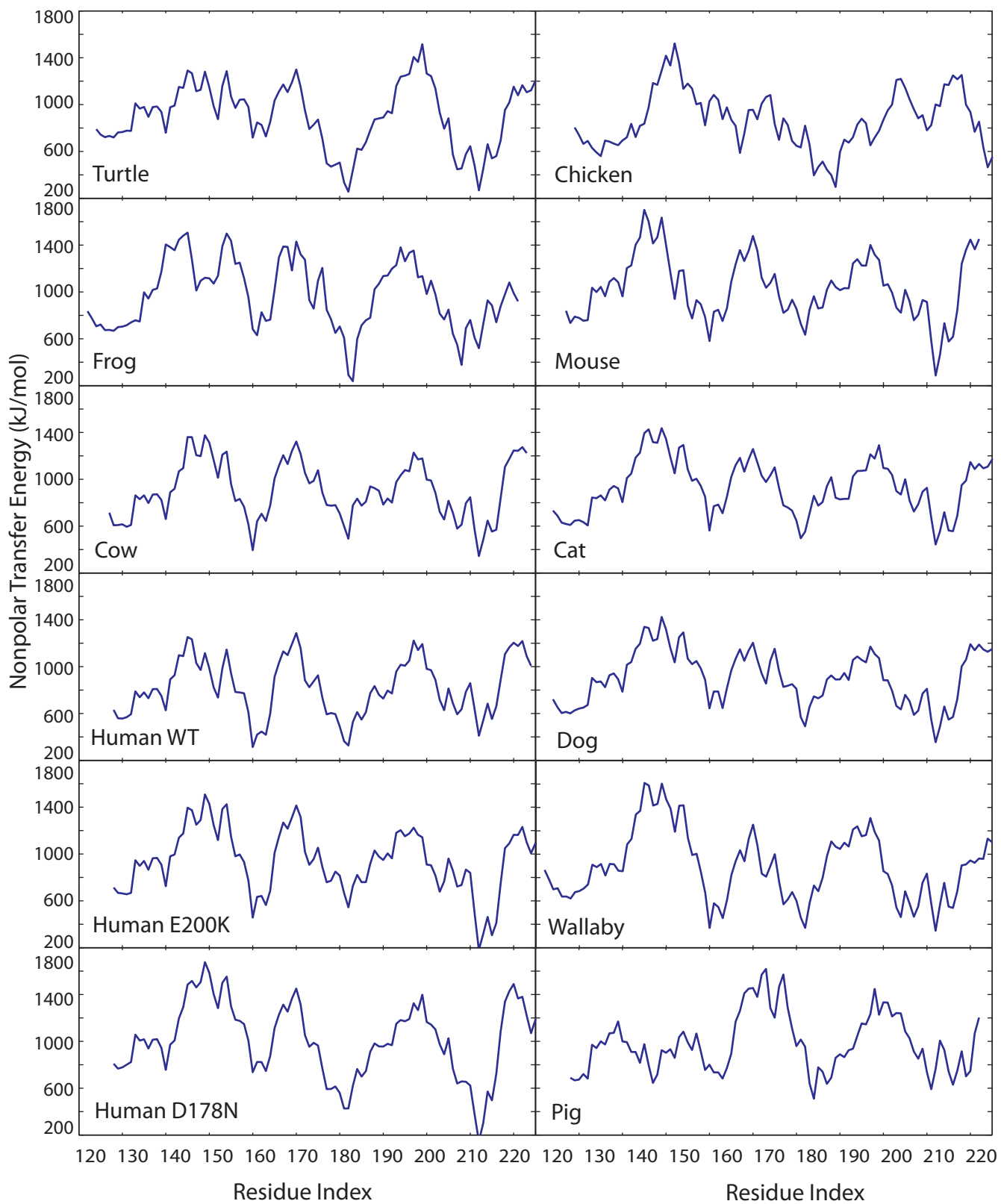
Figure 4: Hydrophobic transfer energies from Equation 4 for seven residue contiguous segments of 12 prion protein structures. The residue index gives the position of the middle residue in each segment.